

PREPARED FOR SUBMISSION TO JCAP

Gravitational waves from a first-order phase transition of the inflaton

Jörn Kersten,^{a,b} Seong Chan Park,^{a,c} Yeji Park,^a Juhoon Son,^a
Liliana Velasco-Sevilla^{d,e}

^aDepartment of Physics and IPAP, Yonsei University,
Seoul 03722, South Korea

^bDepartment of Physics and Technology, University of Bergen,
Postboks 7803, 5020 Bergen, Norway

^cSchool of Physics, Korea Institute for Advanced Study,
85 Hoegi-ro, Seoul 02455, South Korea

^dCenter for Quantum Spacetime, Sogang University, 35 Baekbeom-ro,
Seoul 121-742, South Korea

^eDepartment of Physics, Sogang University,
35 Baekbeom-ro, Seoul 121-742, South Korea

E-mail: jkersten@yonsei.ac.kr, sc.park@yonsei.ac.kr, yeji.park@yonsei.ac.kr,
psiomega@yonsei.ac.kr, lilianak@sogang.ac.kr

Abstract. We explore the production of gravitational waves (GW) resulting from a first-order phase transition (FOPT) in a non-minimally coupled ‘Dark Higgs Inflation’ model. Utilizing a dark sector scalar field as the inflaton, we demonstrate how inflationary dynamics naturally set the stage for observable FOPT. These transitions, influenced by thermal and quantum effects, generate GW spectra potentially detectable by observatories such as LISA, DECIGO, the Cosmic Explorer and the Einstein Telescope. Our study highlights the inflaton’s dual role in cosmic inflation and early Universe phase transitions, presenting a unified framework to probe physics beyond the Standard Model through gravitational wave astronomy.

Contents

1	Introduction	1
2	Dark $U(1)$ model	3
2.1	Lagrangian	3
2.2	Scalar potential	5
2.2.1	Effective potential at finite temperature	5
2.2.2	Effective potential for Dark Higgs Inflation	6
3	Parameter space compatible with inflation and FOPT	7
3.1	First-order phase transitions	7
3.1.1	Benchmark points without fermions	8
3.1.2	Benchmark points with fermions	9
3.2	Inflationary observables	11
4	Conclusions	13
A	One-loop thermally-corrected scalar potential	15
B	Details about FOPT computations	15
C	Formulas for the gravitational wave density	16

1 Introduction

The earliest epochs of the Universe are hidden from direct observation by the opaqueness of the plasma before the formation of the Cosmic Microwave Background radiation (CMB), blocking photon signals from earlier times. Although we aim to detect more penetrating neutrino signals, even neutrinos were in thermal equilibrium and scattering frequently at temperatures above a MeV, preventing us from accessing earlier information. Energy-wise, we are confined by the TeV cap established by the LHC at present, and thus we cannot indirectly access information about the early Universe above the TeV scale. It is, therefore, crucial to explore alternative approaches to detect early Universe signals instead of depending on the slowly advancing energy capacities of colliders alone. Gravitational waves (GW) could be a promising option.

Gravitational wave signals might arise from a variety of early Universe sources [1]. They could originate from the inflationary era as well as from a violent first-order phase transition (FOPT), for instance. The characteristics of such waves will vary depending on their sources, providing opportunities to explore physics in the early Universe beyond the TeV scale. This paper seeks to present a unified framework for cosmic inflation alongside a FOPT, both stemming from the same inflaton field. The observation of a GW signal from this FOPT would be a vital tool for probing the early Universe and offer crucial insights into inflation.

Among the various models for cosmic inflation, Higgs Inflation [2] stands out as an appealing choice due to its simplicity and compatibility with observational data, distinguishing it from other well-known models such as chaotic inflation, power-law inflation, and natural

inflation. The model requires only one modification to the Standard Model (SM): a non-minimal coupling of the Higgs doublet to the Ricci scalar, expressed as $\xi H^\dagger H R$, where ξ is a dimensionless parameter [3, 4]. From the perspective of effective field theory, this non-minimal coupling is natural, as quantum effects will generate it even if $\xi(\mu_c) = 0$ is imposed by hand at a particular scale μ_c . The normalization of the CMB fixes the ratio between the non-minimal coupling parameter and the self-coupling constant at the scale of inflation:

$$\left. \frac{\lambda}{\xi^2} \right|_{\mu_{inf}} \sim 10^{-9}. \quad (1.1)$$

The hierarchy in the ratio is addressed in Critical Higgs Inflation [5, 6], where the self-coupling (λ) of the Higgs becomes small due to the significant influence of the large top quark Yukawa coupling on its renormalization group evolution.

To evaluate the potential significance of the non-minimal coupling at low energy scales, we analyzed higher-dimensional operators, including D=6 and D=8, that emerge at these scales. However, their contributions are insufficient to induce a FOPT, consistent with the findings of [7–15] for EW scale GW production. On the other hand, the R^2 term can play a role in the ultraviolet (UV) completion of Higgs inflation models [16–18]. In these scenarios, the production of gravitational waves and primordial black holes can become significant due to the presence of a new scalar degree of freedom, known as the scalaron, introduced by the R^2 term [19, 20]. In this paper, however, we focus on GW production through a FOPT in a single-field framework, without introducing the scalaron.

In particular, we will consider FOPT occurring well below the inflationary energy scale down to the EW scale. Indeed, the interest in GW produced at the EW scale has exponentially increased due to the many planned and proposed experiments such as the Laser Interferometer Space Antenna (LISA) [21], Einstein Telescope [22], Cosmic Explorer [23], DECIGO [24] and BBO [25] that will be operating in the frequency ranges from about 10^{-5} Hz up to a few Hz, which is the characteristic frequency window associated with the EW scale GW production. To achieve a relatively low-scale FOPT, we extend beyond the SM Higgs inflation framework and consider ‘dark Higgs inflation.’ This involves dark sector particles, including a dark sector scalar (the dark Higgs acting as the inflaton), dark sector fermions, and dark gauge bosons associated with a dark gauge symmetry. Numerous studies have shown that the breaking of dark gauge symmetry can induce an FOPT and generate observable GW [26–31]. Additionally, various models that incorporate dark Higgs fields and dark $U(1)$ symmetry breaking have been proposed [32–34], exploring energy scales ranging from sub-EW to TeV [35]. Some studies have specifically examined the dependence of GW frequencies on the symmetry-breaking scale [27, 36]. While connections between inflation and phase transitions have been investigated [37–39], these works often rely on hybrid models or focus primarily on EW-scale FOPT.

Our work is structured as follows: Sec. 2 introduces the dark $U(1)_X$ model and its scalar potential, including thermal and one-loop corrections relevant to the phase transition. Sec. 3 presents benchmark points for a FOPT and demonstrates compatibility with CMB constraints on inflationary parameters. We conclude in Sec. 4. Various technical details are discussed in appendices.

2 Dark $U(1)$ model

2.1 Lagrangian

In the minimal setup, the dark sector contains a complex scalar ϕ (“Dark Higgs”) charged under a gauge group $U(1)_X$ and the corresponding gauge boson X^μ . The scalar has a non-minimal coupling to gravity determined by the dimensionless parameter ξ , which allows it to act as the inflaton, in analogy to the Higgs Inflation scenario involving the SM Higgs [2]. Thus, the Lagrangian in the Jordan frame is

$$\mathcal{L}_J = \sqrt{-g_J} \left[\frac{\bar{M}_{\text{Pl}}^2}{2} \Omega^2(\phi) R_J + g_J^{\mu\nu} (D_\mu \phi)^\dagger (D_\nu \phi) - \frac{1}{4} g_J^{\mu\rho} g_J^{\nu\sigma} X_{\mu\nu} X_{\rho\sigma} - V_J(\phi) \right], \quad (2.1)$$

where $\bar{M}_{\text{Pl}} = \frac{1}{\sqrt{8\pi G}} \simeq 2.4 \times 10^{18}$ GeV is the reduced Planck mass,

$$\Omega^2(\phi) = 1 + 2\xi \frac{\phi^\dagger \phi}{M_{\text{Pl}}^2} \quad (2.2)$$

is the conformal factor representing the non-minimal coupling, and R_J is the Ricci scalar in the Jordan frame. The remaining quantities are defined as

$$D^\mu \phi = (\partial^\mu + igX^\mu) \phi, \quad (2.3)$$

$$X^{\mu\nu} = \partial^\mu X^\nu - \partial^\nu X^\mu, \quad (2.4)$$

$$V_J(\phi) = -\mu^2 \phi^\dagger \phi + \lambda (\phi^\dagger \phi)^2 = \lambda \left(\phi^\dagger \phi - \frac{v^2}{2} \right)^2 + \text{const.}, \quad (2.5)$$

where for convenience we have chosen the $U(1)_X$ charge equal to one for the scalar. We assume $\mu^2 > 0$, such that the $U(1)_X$ symmetry is broken spontaneously by a vacuum expectation value $v = \mu/\sqrt{\lambda} \ll M_{\text{Pl}}$, which yields a mass $m_X = gv$ for the gauge boson at tree level.

In order to study the impact of fermionic degrees of freedom in the FOPT analysis, we also consider the option of adding n_ψ pairs of chiral fermions ψ_{L_i} and ψ_{R_i} with equal $U(1)$ charges of $\frac{1}{2}$, which ensures anomaly cancellation [40] and allows Yukawa couplings to the scalar,

$$\mathcal{L}_\psi = \sqrt{-g_J} \sum_{i=1}^{n_\psi} \left[\bar{\psi}_{L_i} i \not{D} \psi_{L_i} + \bar{\psi}_{R_i} i \not{D} \psi_{R_i} - \frac{y}{2} (\bar{\psi}_{L_i} \phi \psi_{L_i}^c + \bar{\psi}_{R_i} \phi \psi_{R_i}^c + \text{h.c.}) \right], \quad (2.6)$$

where

$$\not{D} \psi_{L,R_i} = \gamma^m e_m^\mu \left(\partial_\mu + i \frac{g}{2} X_\mu + \omega_\mu \right) \psi_{L,R_i} \quad (2.7)$$

and $\omega_\mu(x)$ is the spin connection.¹ The superscript c denotes charge conjugation. We assume a universal Yukawa coupling y for simplicity. We also assume the potential mass terms $-m \bar{\psi}_{L_i} \psi_{R_i}$ to be irrelevant, i.e., $m \ll v$. After spontaneous symmetry breaking, we obtain $2n_\psi$ Majorana fermions $\psi_{L_i} + \psi_{L_i}^c$ and $\psi_{R_i} + \psi_{R_i}^c$ with mass $m_f = \frac{y}{\sqrt{2}} v$ at tree level.

We have included the coupling to gravity of all particles, but only the gravitational interactions of the scalar will be relevant in the discussion of inflation in the following.

¹Here, we used the Latin index m for the local inertial coordinates $\{\xi^m\}$ and the Greek index μ for the general coordinates $\{x^\mu\}$. Then $\sqrt{-g_J}$ corresponds to the determinant of the vierbein $e_\mu^m = d\xi^m/dx^\mu$.

The purpose of our studies is to determine the conditions under which a strong FOPT that can produce observable GW can take place, and hence we want to explore scales between the Planck mass and much lower energies. For this purpose, we need to take into account the renormalization group (RG) evolution of the couplings in the Lagrangians (2.1) and (2.6) between \overline{M}_{Pl} and the symmetry-breaking scale v at which a FOPT can occur. Using SARAH [41, 42], we obtain the 1-loop RG equations

$$16\pi^2 \mu_R \frac{dg}{d\mu_R} = \frac{n_\psi + 1}{3} g^3, \quad (2.8)$$

$$16\pi^2 \mu_R \frac{dy}{d\mu_R} = (n_\psi + 1) y^3 - \frac{3}{2} g^2 y, \quad (2.9)$$

$$16\pi^2 \mu_R \frac{d\lambda}{d\mu_R} = 20\lambda^2 - 12g^2\lambda + 4n_\psi y^2\lambda + 6g^4 - 2n_\psi y^4 \quad (2.10)$$

above the symmetry-breaking scale ($\mu_R > v$), where μ_R is the renormalization scale.

For $\lambda, y \ll g$, the evolution of the scalar self-coupling is dominated by the gauge interactions, which decrease its value when running from high to low energies. As we have to require a positive value at the symmetry-breaking scale, this leads to a lower bound on λ at the Planck scale. Conversely, given a value of λ yields an upper limit on g . Approximating the r.h.s. of eq. (2.10) to be constant and dominated by $6g^4$, we estimate the running to change λ by

$$\lambda(v) - \lambda(\overline{M}_{\text{Pl}}) \simeq -\frac{6g^4}{16\pi^2} \ln \frac{\overline{M}_{\text{Pl}}}{v} \simeq -0.6 g^4. \quad (2.11)$$

Consequently, we need

$$\lambda(\overline{M}_{\text{Pl}}) \gtrsim 0.6 g^4, \quad (2.12)$$

where the scale at which g is evaluated does not matter much, since g runs fairly slowly.

If the Yukawa coupling dominates the RG evolution, $\lambda, g \ll y$, the relevant term on the r.h.s. of eq. (2.10) is $-2n_\psi y^4$, so λ increases towards smaller energies, and

$$\lambda(v) - \lambda(\overline{M}_{\text{Pl}}) \simeq \frac{2n_\psi y^4}{16\pi^2} \ln \frac{\overline{M}_{\text{Pl}}}{v} \simeq 0.2 n_\psi y^4. \quad (2.13)$$

For large values of the couplings, the running is no longer linear and the above approximations become invalid. Some couplings can become too large for perturbative calculations to be reliable. This is most likely to happen for the scalar self-coupling. For example, for $n_\psi = 1$, $v = 10^{12}$ GeV, and $\lambda, y \ll g$ at that scale, the gauge coupling must be smaller than about 1.4 to ensure a sufficiently small value of λ up to the Planck scale.

If g and y are of similar size, it is possible to combine their effects on the RG evolution to realize small values of λ at both v (as required for a FOPT, see Sec. 3.1) and \overline{M}_{Pl} (as required for Critical Higgs Inflation, see Sec. 3.2). Alternatively, we could add fermions with vectorlike masses larger than v that modify the running but not the PT. Of course, both options require fine-tuning.

We assume a coupling between the dark sector and the SM particles (visible sector) that is sufficiently strong to keep both sectors in thermal equilibrium with a common temperature but sufficiently weak to justify neglecting the impact of SM particles on the dark Higgs effective potential and the phase transition. The latter also ensures that collider searches do not constrain the dark sector for $v \gtrsim 10^4$ GeV. The simplest options for such a coupling are a Higgs portal as well as a kinetic mixing term between the dark gauge boson and the

$U(1)_Y$ gauge boson. After the phase transition, this coupling allows the remaining dark sector particles to decay to SM particles.² Hence, the cosmological evolution at temperatures sufficiently below the $U(1)_X$ symmetry breaking scale is unchanged compared to the SM.

2.2 Scalar potential

2.2.1 Effective potential at finite temperature

We write the complex scalar in terms of two real fields,

$$\phi = \frac{1}{\sqrt{2}}(h + i\chi). \quad (2.14)$$

By gauge invariance, the effective potential depends only on

$$\phi_c^\dagger \phi_c = \frac{1}{2}(h_c^2 + \chi_c^2),$$

where the subscript c denotes a classical field. Consequently, we can set $\chi_c = 0$ without loss of generality and write the effective potential as a function of h_c . Then the effective potential at finite temperature for the dark sector is given by

$$V(h_c, T) = V_{\text{tree}}(h_c) + \sum_{i=h,f,g,\chi} (V_{i,1l}(h_c) + V_{i,\text{th}}(h_c, T)), \quad (2.15)$$

where the indices h, f, g, χ refer to the scalar, fermion, gauge boson and Nambu-Goldstone boson contributions, respectively. The tree-level potential is given by

$$V_{\text{tree}}(h_c) = -\frac{\mu^2}{2}h_c^2 + \frac{\lambda}{4}h_c^4. \quad (2.16)$$

The function $V_{i,1l}(h_c)$ is the 1-loop correction at zero temperature [43] and $V_{i,\text{th}}(h_c, T)$ is the 1-loop correction at finite temperature [44, 45], are given for completeness in Eq. (A.2) of App. A. These functions depend on the field-dependent masses

$$\begin{aligned} m_h^2(h_c) &= -\mu^2 + 3\lambda h_c^2, \\ m_\chi^2(h_c) &= -\mu^2 + \lambda h_c^2, \\ m_g^2(h_c) &= g^2 h_c^2, \\ m_f^2(h_c) &= \frac{y^2}{2} h_c^2. \end{aligned} \quad (2.17)$$

The 1-loop functions also depend on the bosonic and fermionic degrees of freedom

$$n_g = 3, \quad n_h = 1, \quad n_\chi = 1, \quad n_f = -4n_\psi, \quad (2.18)$$

where the latter are defined as a negative number for convenience. Of course, $n_\psi = 0$ for the case without fermions.

²If one of the dark sector particles is stable, it is a dark matter candidate. We leave an exploration of this option for future work.

2.2.2 Effective potential for Dark Higgs Inflation

The calculation of the scalar potential during the inflationary phase proceeds in analogy to the well-known Higgs Inflation scenario [2, 46]. We include it here for clarity and to fix the notation. For brevity, we set $\bar{M}_{\text{Pl}} = 1$ in this section. Starting from the Jordan frame Lagrangian (2.1), the Lagrangian in the Einstein frame can be obtained by the Weyl transformation

$$g_{J\mu\nu} \rightarrow g_{\mu\nu} \equiv \Omega^2 g_{J\mu\nu}, \quad (2.19)$$

$$g_J^{\mu\nu} \rightarrow g^{\mu\nu} \equiv \Omega^{-2} g_J^{\mu\nu}, \quad (2.20)$$

$$g_J = \det(g_{J\mu\nu}) \rightarrow g = \Omega^8 g_J, \quad (2.21)$$

$$R_J = g_J^{\mu\nu} R_{J\mu\nu} \rightarrow R = \Omega^{-2} R_J + \frac{3}{2} g^{\mu\nu} (\partial_\mu \ln \Omega^2) (\partial_\nu \ln \Omega^2) - 3 \square \ln \Omega^2, \quad (2.22)$$

where the subscript J refers to quantities in the Jordan frame, and quantities without this subscript are understood to be in the Einstein frame. The last term in Eq. (2.22) is a total divergence and can be dropped. Using unitary gauge, $\phi = \frac{1}{\sqrt{2}} h$, and switching to the canonically normalized field ζ , the scalar Lagrangian becomes

$$\mathcal{L}_\zeta = \sqrt{-g} \left[\frac{1}{2} R + \frac{1}{2} (\partial_\mu \zeta) (\partial^\mu \zeta) - V(\zeta) + (\text{gauge interactions}) \right], \quad (2.23)$$

where we have identified the potential in the Einstein frame as

$$V(\zeta) = \frac{V_J(h(\zeta))}{\Omega^4(h(\zeta))} = \frac{\frac{\lambda}{4} (h^2 - v^2)^2}{(1 + \xi h^2)^2} \quad (2.24)$$

and where the canonically normalized scalar is obtained via

$$\zeta = \int_0^h dh' \sqrt{\frac{6\xi^2 h'^2}{\Omega^4(h')} + \frac{1}{\Omega^2(h')}}. \quad (2.25)$$

The integration can be performed in a straightforward way,

$$\begin{aligned} \zeta &= \sqrt{\frac{1}{\xi} + 6} \sinh^{-1} \left(h \sqrt{\xi(6\xi + 1)} \right) - \sqrt{6} \tanh^{-1} \left(\frac{\sqrt{6} h \xi}{\sqrt{h^2 \xi(6\xi + 1) + 1}} \right) \\ &\simeq \begin{cases} h & , \quad h \ll \frac{1}{\sqrt{\xi}} \\ \sqrt{6 + \frac{1}{\xi}} \ln(h \sqrt{\xi}), & h \gg \frac{1}{\sqrt{\xi}}. \end{cases} \end{aligned} \quad (2.26)$$

Then the potential in the Einstein frame can be expressed in the two regimes as

$$V(\zeta) \simeq \begin{cases} \frac{\lambda}{4} \zeta^4 & , \quad v \ll h \sqrt{\xi} \ll 1 \\ \frac{\lambda}{4\xi^2} \left(1 + \exp \left(-\frac{2\zeta}{\sqrt{6 + 1/\xi}} \right) \right)^{-2} & , \quad h \sqrt{\xi} \gg 1. \end{cases} \quad (2.27)$$

Consequently, the potential becomes flat for large field values, which enables slow-roll inflation.

3 Parameter space compatible with inflation and FOPT

3.1 First-order phase transitions

Our final goal is to identify concrete conditions for the parameter space where we can achieve a strong FOPT in general dark sector gauge models, but we leave this discussion for later work [47]. As a proof of principle, we present here several benchmark points for which a FOPT leading to measurable GW can occur.

FOPT can proceed via different processes: nucleation, expansion, collision and merger of bubbles of the broken phase. The way these processes can source GW is quite varied. If the phase transition occurs only in vacuum, the only source of GW is the collision of the bubble walls and the GW density as a function of the frequency can be expressed in terms of the envelope approximation [48]. If the scalar bubbles expand instead in a hot plasma, the plasma friction will slow down the expansion of the walls and so most of the energy released by the transition will be transferred from the scalar field into the plasma, making the contribution to GW from the scalar field subdominant in comparison to that of the plasma. Numerical simulations of this process on a 3D lattice have shown that the energy-momentum tensor of the fluid after bubble collisions corresponds to an ensemble of sound waves [49, 50] and that this process dominates over all over the others in the case of the hot plasma. This dominance is the so-called acoustic phase. A competing source of GW is turbulence [51–55] created in the plasma, and in fact for very strong transitions the acoustic phase turns over into a turbulent stage which continues to produce gravitational radiation until it decays. In order to determine the dependence of the GW on the parameters of the phase transition and on the frequency it is necessary to capture the shock waves in the plasma and for this numerical simulations are needed. We use up-to-date GW templates (fits in terms of frequency power laws and parameters of the theory) from 3D lattice simulations [49, 56–59]. Simulations and fits of the GW density are an active line of research and continuously improving. The useful information is to locate the peak frequency and to establish an order of magnitude of the GW density. One crucial ingredient of the FOPT is the parameter α , which is the ratio of the vacuum energy density released in the transition and of the plasma energy density in the symmetric phase. For our case,

$$\alpha = \frac{1}{\rho_{\text{rad}}} \left[\Delta V(h_c, T) - T \frac{dV(h_c, T)}{dT} \right] \Big|_{T=T_n}, \quad (3.1)$$

which turns out to be the ratio of the latent heat to the radiation density in the case of GW production during the radiation-dominated era.³ Here $\Delta V(h_c, T)$ is the difference of the effective potential of Eq. (2.15) between the true minimum and the false minimum and T_n is the nucleation temperature. The derivative is evaluated at the true potential minimum.

For our study, we restrict ourselves to benchmark points with $\alpha \sim 0.1$, a value which is safe since the radiation density increases relative to the GW density as the Universe cools and particles annihilate. Furthermore, the lattice simulations on which the templates that we use are valid only in the $\alpha \lesssim 0.1$ regime [49, 56–58].⁴ For completeness, we include the formulas we use in App. C. Gravitational wave frequency density templates for $\alpha > 1$ exist but they require more knowledge about the difference between the reheating temperature and the nucleation temperature. For the case of small α and the barrier of the potential produced

³The observed upper limit on the effective number of neutrino species N_{eff} places an upper limit on α .

⁴Recent templates have been obtained in [60] but for weak ($\alpha = 0.0046$) and intermediate ($\alpha = 0.05$) FOPT in a hybrid 1D lattice-analytical approach. We comment on this in App. C.

BP	$g(v)$	$\lambda(v)$	v/GeV	T_0/v	T_c/v	T_n/v	α	β/H_*
BP1	0.95	10^{-3}	10^{12}	0.068	0.37	0.11	0.94	1.3×10^2
BP2			10^9			0.13	0.45	1.5×10^2
BP3			10^6			0.16	0.25	1.9×10^2
BP4			10^3			0.18	0.16	2.4×10^2

Table 1. Benchmark points leading to a FOPT for the case without fermions ($n_\psi = 0$).

mainly by thermal effects, the reheating temperature and the nucleation temperature can be safely identified with each other. Another crucial parameter in the computation of GW density from FOPT is the beta parameter

$$\beta = H_* T \frac{d}{dT} \left(\frac{S_3}{T} \right) \Big|_{T=T_n \approx T_*}, \quad (3.2)$$

which quantifies how fast or slow the FOPT occurs. Here T_* is the temperature of the thermal bath and S_3 is the 3D action

$$S_3[h_c(r), T] = 4\pi \int_0^\infty r^2 dr \left[\frac{1}{2} \left(\frac{dh_c(r)}{dr} \right)^2 + V(h_c(r), T) \right], \quad (3.3)$$

where r represents the radius of the bubble and $h_c(r)$ the instanton solution.

3.1.1 Benchmark points without fermions

We are interested in finding values of g and λ for which observable GW spectra can be produced as a result of a FOPT. In the case of no fermions, we find a FOPT leading to acceptable GW parameters for $g(v) = 0.95$ and $\lambda(v) = 10^{-3}$, where v is close to the scale at which the FOPT occurs. In Tab. 1 we present four benchmark points (BP) for this case, which differ in the value of v . We also show the characteristic temperatures of the FOPT, T_0 , T_c and T_n , which are, respectively, the temperature at which $\partial^2 V(h_c, T)/\partial h_c^2 = 0$ at the origin, the critical temperature (at which the two minima are degenerate) and the nucleation temperature (the temperature at which one bubble is nucleated per Hubble horizon on average, see Eq. (B.2)). Finally, the parameters α and β/H_* , defined in Eqs. (3.1) and (3.2), are given. We refer to App. B for details of the computation.

The way the 1-loop corrections contribute to the effective potential (2.15), at zero temperature and at finite temperature, are shown in Fig. 4. Given the small size of λ , the tree-level contribution is subdominant and the 1-loop contributions and the thermal contributions are necessary for the formation of the potential barrier,⁵ as can be seen in the bottom left plot of Fig. 4. The expansion of $J_b(m_i^2(h_c)/T^2)$ in terms of powers and logarithms of $m_i^2(h_c)/T$ given in Eq. (A.2) is the high-temperature approximation and even if it does not match entirely the shape of the complete thermal corrections (see top and middle plots of Fig. 4), it is useful to understand the behavior of the barrier. In this case, both the cubic and logarithmic contributions are important to produce a barrier. As these contributions are proportional to g^3 and g^4 , respectively, both the barrier height and α increase significantly with increasing gauge coupling. In Tab. 1 we show the FOPT parameters that we find for our choice of parameters (λ and g for different scales: $v/\text{GeV} \in \{10^3, 10^6, 10^9, 10^{12}\}$).

⁵Note that in this case the fact that 1-loop contributions can overcome the tree level is natural and we are in a regime where 1-loop contributions are reliable since λ is chosen to be small.

As the quantity S_3/T is dimensionless (cf. Eq. (3.3)), we can compute everything related to the phase transition in terms of dimensionless quantities, except for T_n , which depends on the probability of nucleation, represented by Eq. (B.2). Note the factor T^5 in the denominator of the integral in Eq. (B.2); when the symmetry-breaking scale v increases, the T^{-5} suppression becomes more severe and makes it more difficult for the integral between T_n and T_c to reach an $\mathcal{O}(1)$ value, which is required for completing the phase transition. Thus, increasing v causes a decrease of T_n/v ; if v becomes too large, T_n approaches T_0 (where the potential barrier disappears) and a FOPT is not feasible.

In Fig. 1 we show the GW densities we obtain for the benchmark points of Tab. 1 by summing the contributions from sound waves and turbulence given in Eq. (C.1) and Eq. (C.4), respectively. We plot each of the benchmark points with three different bubble wall velocities, v_w , since this quantity dominates the uncertainty in the determination of the GW spectrum, as we explain in App. B and C.

Most importantly, the choice of the symmetry-breaking scale determines the peak frequency of the GW spectrum. The peak height decreases with decreasing v , reflecting the decrease of α . The shape of the spectrum is very similar for all benchmark points.

The figure also displays the current (for the case of LIGO [61]) and expected sensitivities for different experiments: AION [62], LISA [63], Einstein Telescope (ET) [22], Cosmic Explorer (CE) [23], DECIGO [24], BBO [25], SOGRO [64] and a proposed resonant detector [65] operating in the $(10^6, 10^9)$ Hz frequency range. SOGRO is a superconducting tensor detector for mid-frequency GW proposed to fill the gap between LISA and LIGO. In addition, we include the current Big Bang Nucleosynthesis (BBN) bound as well as a forecasted [66] improved bound, which is achievable with future satellite experiments such as CORe [67] and EUCLID [68].

As is well known, GW from FOPT around $v = 10^3$ GeV are expected to peak in the sensitivity range of LISA, as we see from the GW density on the left of the plot in Fig. 1. If $v = 10^3$ GeV, the dark sector can be constrained by LHC searches, in particular invisible Higgs decays into the Dark Higgs, whose mass is about 45 GeV in this case. The relevant parameter is the quartic coupling between the SM Higgs and the Dark Higgs (Higgs portal), whose value can be adjusted rather freely in our scenario. For fairly large kinetic mixing between the X^μ and the SM $U(1)_Y$ gauge boson, the new vector state can also be accessible.

For the case of $v = 10^6$ GeV, CE has the potential to observe the signal. For $v = 10^9$ GeV, future ground-based detectors (not shown in the figure) can probe the relevant area, in principle. For the case of $v = 10^{12}$ GeV, resonant detectors appear promising, which have recently been contemplated as a way to probe the so-called *ultra-high-frequency* region (UHF). We can see that our BP1 lies precisely in the resonant region of the detector proposed in [65].

3.1.2 Benchmark points with fermions

Now we turn to the case with fermions. As we can see from Eq. (A.2) and the expansion of J_f in the regime of $m_i^2(h_c)/T^2 \ll 1$, the fermion contribution to the effective potential does not contain a cubic term and therefore fermions do not enhance the barrier. In Fig. 4 we show the exact thermal behavior along with different approximations and contributions. As opposed to the case of no fermions, the high-temperature approximation is not a good approximation for the complete duration of the phase transition, as the temperature corrections are led mainly by the logarithmic term and to some extent the linear term.

Combining the effects of gauge bosons and fermions on the RG evolution of the scalar self-coupling, it is possible to arrive at $\lambda = 0$ at the Planck scale. In Tab. 2 we show

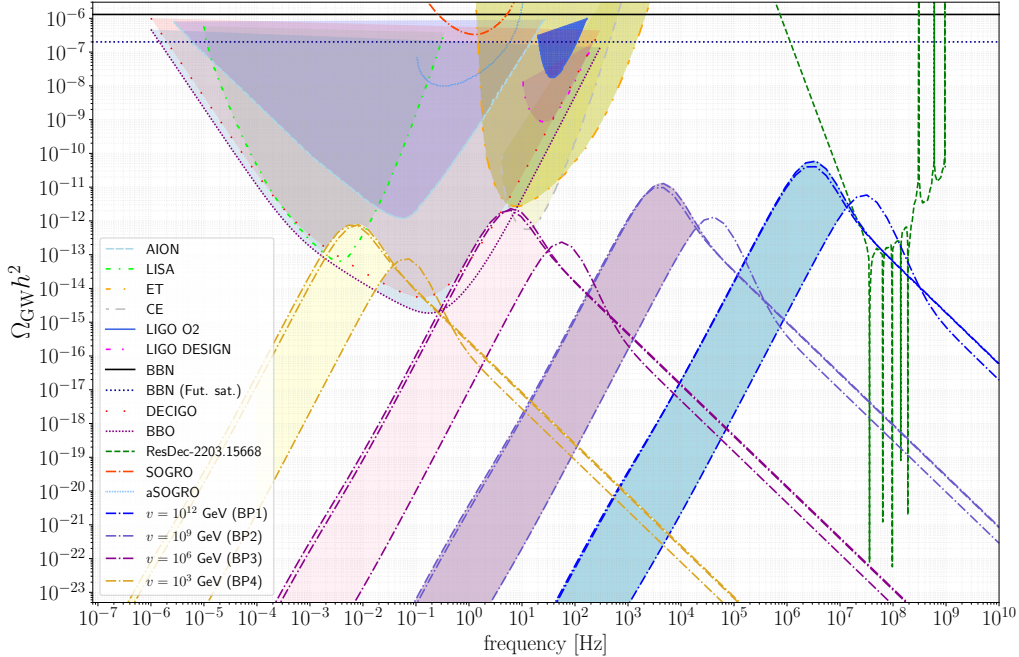


Figure 1. Gravitational wave spectra for the benchmark points BP1 to BP4 (from right to left), which are defined in Tab. 1 and correspond to $v = (10^{12}, 10^9, 10^6, 10^3)$ GeV, respectively. We remind the reader that the formulas for GW have been tested in a regime $\alpha \lesssim 0.1$. The value of α obtained for BP1 ($v = 10^{12}$ GeV) is close to 1, so the result must be taken with caution. For every case we have plotted three bubble wall velocities, corresponding, from left to right, to $v_w = 1$, $v_w = v_w^d$ (the detonation velocity) and $v_w = 0.1$. We note that for some of the cases the first two lines are indistinguishable due to the proximity of v_w^d to 1.

BP	$g(v)$	$\lambda(v)$	$y(v)$	v/GeV	T_0/v	T_c/v	T_n/v	α	β/H_*
BP5	0.76	10^{-3}	0.97	10^{12}	0.067	0.11	0.075	0.10	9.1×10^2
BP6	0.54	10^{-3}	0.70	10^{12}	0.094	0.13	0.10	0.070	1.7×10^3
BP7	0.35	10^{-3}	0.47	10^{12}	0.14	0.16	0.15	0.024	3.9×10^3

Table 2. Benchmark points with $n_{\psi} = 1$ and $\lambda(\overline{M}_{\text{P}1}) \approx 0$, which are shown in Fig. 2.

three different benchmark points realizing this possibility for three different choices of gauge and Yukawa couplings at the symmetry-breaking scale $v = 10^{12}$ GeV. Of course, the initial conditions have to be tuned with a higher precision than given in the table. Besides, the exact location where λ reaches zero is sensitive to higher loop orders. However, these complications do not change the fact that $\lambda(\overline{M}_{\text{P}1}) = 0$ is possible *in principle* and have no impact on the FOPT and the resulting GW.

The corresponding GW densities are shown in Fig. 3, along with the reach of planned and proposed experiments. Here we plot only the GW density profile that corresponds to the detonation bubble wall velocity v_w^d (see App. C) in order not to overcrowd the region about the density profiles. As the values of the Yukawa and gauge couplings are different, the

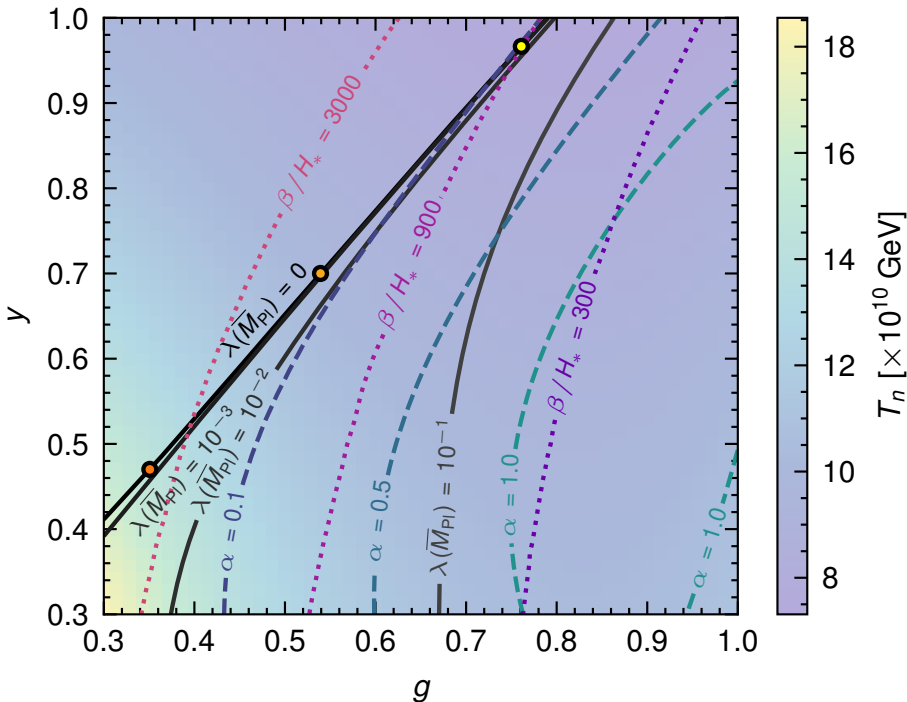


Figure 2. Parameter space in the $(g-y)$ plane at the scale of 10^{12} GeV. The solid lines represent $\lambda(\overline{M}_{\text{Pl}})$ contours for values $\{0, 10^{-3}, 10^{-2}, 10^{-1}\}$, while the dotted and dashed lines show β/H_* contours (3000, 900, 300) and α contours (0.1, 0.5, 1.0), respectively. The benchmark points BP5–BP7 defined in Tab. 2 are denoted by circle markers. The background color gradient represents the nucleation temperature T_n in units of 10^{10} GeV.

corresponding nucleation temperatures are different. Interestingly, the GW density profiles for these cases peak in the region of sensitivity of the resonant detector proposed in [65]. Their height is smaller than in the case without fermions since the gauge coupling is smaller.

We could in principle look for benchmark points at lower scales than $v = 10^{12}$ GeV, as in the case with fermions. However, since the lower the scale the more difficult it is to obtain a large peak amplitude, we do not present them. The qualitative behavior is the same as without fermions, i.e., the peak frequency decreases for decreasing v . The main importance of the case with fermions is that we can drive to zero the value of λ at \overline{M}_{Pl} .

3.2 Inflationary observables

As discussed in Sec. 2.2.2, the scalar potential in the Einstein frame, given in Eq. (2.27), has an asymptotic plateau in the large-field limit. Putting back the Planck mass,

$$V(\zeta) \approx \frac{\lambda \overline{M}_{\text{Pl}}^4}{4\xi^2} \left(1 + \exp\left(-\frac{2\zeta/\overline{M}_{\text{Pl}}}{\sqrt{6+1/\xi}}\right) \right)^{-2} \approx \frac{\lambda \overline{M}_{\text{Pl}}^4}{4\xi^2}, \quad \zeta \gg \overline{M}_{\text{Pl}}/\sqrt{6+1/\xi}. \quad (3.4)$$

This plateau is responsible for the slow-roll inflationary dynamics, which enables the exponential expansion of the Universe. The slow-roll parameters are expressed in terms of the

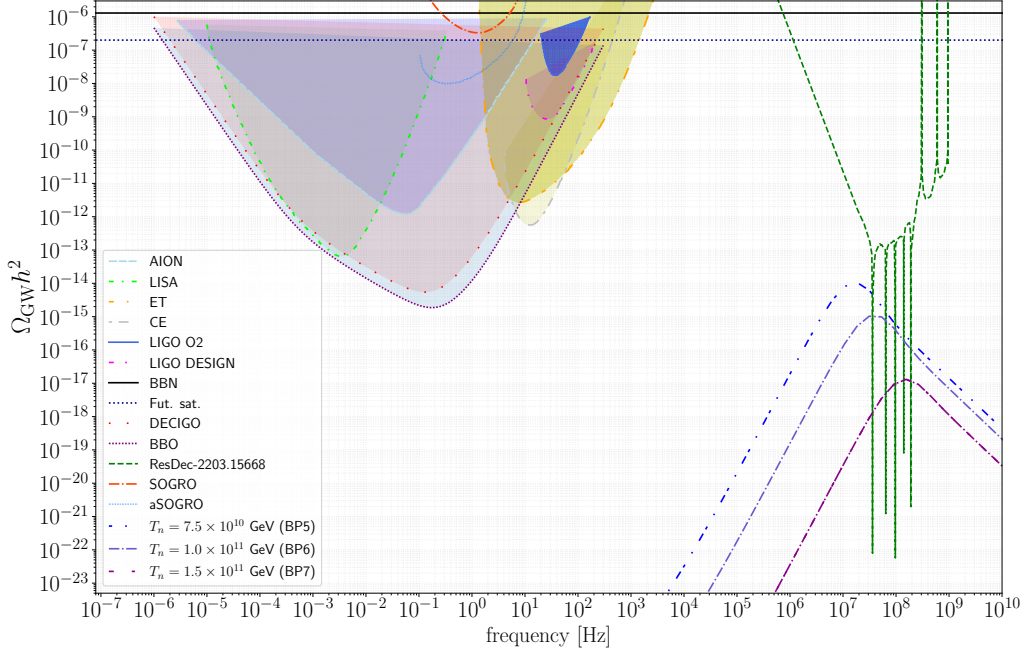


Figure 3. Gravitational wave spectra for the cases of Tab. 2, that is, including a fermion pair. We choose three benchmark points (BP5–BP7) along the line $\lambda(\overline{M}_{\text{Pl}})=0$ of Fig. 2. For all these cases, $v = 10^{12}$ GeV but due to the different gauge couplings, the resulting nucleation temperature T_n is different.

Einstein-frame potential and the canonically normalized field ζ ,

$$\varepsilon = \frac{\overline{M}_{\text{Pl}}^2}{2} \left(\frac{dV/d\zeta}{V} \right)^2 \approx \frac{8\xi}{1+6\xi} \exp\left(-\frac{4\zeta/\overline{M}_{\text{Pl}}}{\sqrt{6+1/\xi}} \right), \quad (3.5)$$

$$\eta = \overline{M}_{\text{Pl}}^2 \frac{d^2V/d\zeta^2}{V} \approx -\frac{8\xi}{1+6\xi} \exp\left(-\frac{2\zeta/\overline{M}_{\text{Pl}}}{\sqrt{6+1/\xi}} \right). \quad (3.6)$$

In the slow-roll framework, we can relate the inflationary observables with the slow-roll parameters and the potential at the pivot scale ζ_* setting $N_* = \int_{\zeta_e}^{\zeta_*} d\zeta/(\overline{M}_{\text{Pl}}\sqrt{2\varepsilon}) = 60$ with $\max(\varepsilon, |\eta|)_{\zeta_e} = 1$ at the end of inflation. The observables are conveniently related to the number of e -foldings as

$$n_s = 1 - 6\varepsilon_* + 2\eta_* \approx 1 - \frac{2}{N_*} - \frac{9}{2N_*^2} \approx 0.965, \quad (3.7)$$

$$r = 16\varepsilon_* \approx \frac{12}{N_*^2} \approx 0.003, \quad (3.8)$$

where we took $\zeta_* \ll \zeta_e$ and neglected the correction $1/(6\xi N_*^2) \lesssim 4 \times 10^{-4}$ for $\xi \gtrsim 1$. These values are in excellent agreement with the Planck2018 results [69], $n_s = 0.965 \pm 0.004$ (for $k_* = 0.05 \text{ Mpc}^{-1}$) and $r < 0.035$ (95% CL), as in conventional Higgs Inflation models. The

BP	$g(\overline{M}_{\text{Pl}})$	$\lambda(\overline{M}_{\text{Pl}})$	$y(\overline{M}_{\text{Pl}})$	n_ψ	ξ
BP1	0.98	0.37	-	0	3.1×10^4
BP2	0.99	0.57	-	0	3.8×10^4
BP3	1.00	0.92	-	0	4.9×10^4
BP4	1.02	2.22	-	0	7.5×10^4
BP5	0.79	≈ 0	1.10	1	$\mathcal{O}(1)$
BP6	0.55	≈ 0	0.74	1	$\mathcal{O}(1)$
BP7	0.35	≈ 0	0.48	1	$\mathcal{O}(1)$

Table 3. Model parameters at \overline{M}_{Pl} . BP1–BP4 correspond to the case of no fermions and BP5–BP7 to the case of $n_\psi = 1$.

CMB normalization provides a condition for λ/ξ^2 ,

$$A_s = \frac{1}{24\pi^2} \frac{V_*}{\varepsilon_*} \approx \frac{\lambda(\overline{M}_{\text{Pl}}) N_*^2}{72\pi^2 \xi^2}. \quad (3.9)$$

Using $A_s = (2.098 \pm 0.023) \times 10^{-9}$ [69], we conclude

$$\frac{\lambda(\overline{M}_{\text{Pl}})}{\xi^2} \approx 3.9 \times 10^{-10} \quad (3.10)$$

for $N_* = 60$ e -foldings.

We show the resulting values of ξ for our seven benchmark points in Tab. 3, together with the values of the other couplings at \overline{M}_{Pl} .

If we insist that the naïve cut-off scale of the model, given by $\overline{M}_{\text{Pl}}/\xi$ or $\overline{M}_{\text{Pl}}/\sqrt{\xi}$ [70–72], not lie much below the Planck scale, we are motivated to consider the conformal scenario with $\lambda(\overline{M}_{\text{Pl}}) \ll 1$, which is analogous to the Critical Higgs Inflation scenario with the SM scalar [5, 6]. In this case, small values of ξ are consistent with Eq. (3.10). It is realized at the benchmark points BP5–BP7, where the RG running of the self-coupling λ is affected by a large negative contribution from fermions, as discussed above.

The precise value of λ at the pivot scale is slightly modified by the positive contribution from the gravitational interactions (see, e.g., [3]).

4 Conclusions

In this study, we explored an extension of the Standard Model incorporating a simple dark sector with a $U(1)_X$ gauge symmetry. We identified a compelling scenario where a single scalar field drives both slow-roll inflation and spontaneous symmetry breaking, leading to the production of gravitational waves (GWs). The predicted GW spectrum peaks at frequencies between 10^{-2} Hz and 10^8 Hz, making it accessible to future GW observatories.

Inflation in this model is realized analogously to the Higgs inflation scenario, but with the Standard Model Higgs replaced by the Dark Higgs, which breaks the $U(1)_X$ symmetry. Notably, the model accommodates the particularly appealing case of Critical Dark Higgs Inflation, where the inflaton field’s self-coupling at the inflationary scale is fine-tuned via renormalization group running. This behavior emerges from significant fermionic contributions in loop corrections, while the bosonic contributions from gauge fields ensure a viable first-order phase transition (FOPT) at a lower energy scale, producing detectable GWs.

Our proposed scenario offers a novel pathway to probe inflation through GW observations, complementing traditional searches for GWs produced during inflation. Additionally, the dark sector naturally provides a candidate for dark matter, addressing another critical problem in astroparticle physics. While we focused on a simple $U(1)_X$ model, this framework can be extended to larger gauge groups. Larger groups enable faster parameter evolution through renormalization group running and can create higher potential barriers, potentially leading to stronger FOPTs and enhanced GW signals. Such extensions open further opportunities for exploring the interplay between cosmology, particle physics, and gravitational wave astronomy.

Acknowledgments

We thank Vincenzo Branchina, Injun Jeong and Stefano Scopel for useful discussions. J.K. thanks *Star Trek The Next Conversation* for inspiration – 5 stars out of 5. The work of L.V.S. is supported by the National Research Foundation of Korea (NRF) grant no. RS-2023-00273508. S.C.P. was supported by the NRF grant funded by the Korean government (MSIT) no. RS-2023-00283129 and RS-2024-00340153. J.K. is supported by the NRF’s *Brain Pool* program under grant no. RS-2023-00283129.

A One-loop thermally-corrected scalar potential

For completeness we give here the 1-loop and thermal corrections [43–45] to the potential, which is a function of the classical scalar field h_c .

$$\begin{aligned}
V_{i,1l}(h_c) &= \frac{n_i}{64\pi^2} m_i^4(h_c) \left(\ln \frac{|m_i^2(h_c)|}{v^2} - C_i \right), \\
V_{i,\text{th}}(h_c, T) &= \begin{cases} \frac{n_i}{2\pi^2} T^4 J_b(x), & i = h, g, \chi \\ \frac{n_i}{2\pi^2} T^4 J_f(x), & i = f \end{cases}, \quad x \equiv \frac{m_i(h_c)}{T}, \\
J_b(x) &= \Re \int_0^\infty dy y^2 \ln \left[1 - e^{-\sqrt{y^2+x^2}} \right], \\
&\stackrel{\text{High}}{\approx} -\frac{\pi^4}{45} + \frac{\pi^2}{12} x^2 - \frac{\pi}{6} x^3 - \frac{1}{32} x^4 \ln \frac{|x^2|}{a_B}, \quad |x^2| \ll 1, \\
J_f(x) &= \Re \int_0^\infty dy y^2 \ln \left[1 + e^{-\sqrt{y^2+x^2}} \right], \\
&\stackrel{\text{High}}{\approx} \frac{7\pi^4}{360} - \frac{\pi^2}{24} x^2 - \frac{1}{32} x^4 \ln \frac{|x^2|}{a_F}, \quad x^2 \ll 1, \\
a_B &= 223.1, \quad a_F = 13.94.
\end{aligned} \tag{A.1}$$

The index i takes the values h, f, g, χ for the scalar, fermion, gauge boson, and Nambu-Goldstone boson contributions, respectively. The field-dependent masses were already given in the main text in Eq. (2.17). Also, $C_i = 5/6$ for gauge bosons and $C_i = 3/2$ for scalars and fermions. The degrees of freedom n_g, n_h, n_χ and n_f have been defined in Eq. (2.18).

Note that for $h_c < v$, the field-dependent scalar masses can be imaginary. In this case, V_{1l} approximates the *modified* effective potential, whose real part determines the energy density and is thus the relevant quantity for the phase transition [10, 73, 74]. Accordingly, we have defined $V_{i,1l}$ and $V_{i,\text{th}}$ as real functions.

B Details about FOPT computations

After calculating the effective potential, with 1-loop corrections at zero temperature and finite-temperature corrections, the decay rate of the false vacuum, $\Gamma(T)$ has to be computed. $\Gamma(T)$ can be obtained from [45, 75, 76]

$$\Gamma(T) \simeq \max \left[T^4 \left(\frac{S_3}{2\pi T} \right)^{\frac{3}{2}} \exp(-S_3/T), R_0^{-4} (S_4/2\pi)^2 \exp(-S_4) \right], \tag{B.1}$$

where R_0 represents the size of the nucleation bubble in four dimensions, S_3 and S_4 are, respectively, the Euclidean actions in three and four dimensions corresponding to the $O(3)$ and $O(4)$ symmetric tunneling configurations, referred to as bounce solutions. In all cases we have studied, the first term in the brackets turns out to be the larger one. Approaches to compute 1-loop functional determinants around spherical symmetric backgrounds, providing the next-to-leading-order correction to the bubble nucleation rates and hence removing the uncertainties in the expression of $\Gamma(T)$ above exist [77]. However, the purpose of our work is to establish a proof of concept of the existence of a parameter space where a non-minimally coupled inflaton to gravity leads to observable GW from a FOPT and hence we leave a more accurate computation of $\Gamma(T)$ for future work. Furthermore, the precise value of the

prefactor in the nucleation rate, Eq. (B.1), is not critically important due to the dominance of the exponential term [78]. Based on this reasoning, one can simplify the calculations by setting the term $(S_3/2\pi T)^{3/2}$ to 1.

Once $\Gamma(T)$ is computed, the nucleation temperature T_n can be determined by calculating the temperature at which the average number of bubbles nucleated per Hubble horizon is of order 1,

$$N(T_n) = \left(\frac{3\overline{M}_{\text{Pl}}}{\pi}\right)^4 \left(\frac{10}{g_*}\right)^2 \int_{T_n}^{T_c} \frac{dT}{T^5} \left(\frac{S_3}{2\pi T}\right)^{3/2} \exp(-S_3/T) \sim 1, \quad (\text{B.2})$$

assuming the PT to occur in the radiation-dominated era. All results presented in Sec. 3.1 were obtained setting $N(T_n) = 1$. The parameter g_* is the effective number of relativistic degrees of freedom (d.o.f.). In our case, apart from the SM d.o.f. $g_{*,\text{SM}} = 106.75$, we have ϕ (a complex scalar), the $U(1)$ gauge boson, and $2n_\psi$ Majorana fermions, so

$$g_* = g_{*,\text{SM}} + 4 + \frac{7}{2}n_\psi. \quad (\text{B.3})$$

After T_n is computed, the parameters α and β follow from Eqs. (3.1) and (3.2). We have determined these parameters with our own codes based on the bounce solutions calculated by `CosmoTransitions` [79].

The computation of α and β/H_* is affected by numerical uncertainties, both from intrinsic numerical algorithms and from the expression in Eq. (B.2). In fact, varying the right-hand side of Eq. (B.2) between 0.1 and 10, we find a variation of T_n/v , α , and β/H_* at the percent level. These uncertainties, however, are subdominant with respect to the value of the bubble wall velocity v_w .⁶ As we explain in more detail in App. C, we choose to present our results with three values of v_w to chronicle this uncertainty.

C Formulas for the gravitational wave density

The density of GW is controlled by the following parameters: T_n , α , β , the sound speed, c_s , the bubble wall speed v_w , and the efficiency factors κ_ν , and ϵ . In terms of these parameters, we can use the well-known formulas [49, 56] for sound wave and turbulence contributions [57, 58] when the barrier is mainly of thermal origin, that is, it disappears in the limit of $T \rightarrow 0$ and the 1-loop gauge coupling contributions are not negligible. This is the so-called case of *non-runaway bubbles*. In this case, the main contributions come from the sound waves and the magnetohydrodynamic (MHD) turbulence of the plasma. The red-shifted contribution to the GW density from sound waves today is given by

$$\Omega_{\text{sw}} h^2(f) = 2.65 \times 10^{-6} H_* \tau_{\text{sw}} \left(\frac{\beta}{H_*}\right)^{-1} v_w \left(\frac{\kappa_\nu \alpha}{1 + \alpha}\right)^2 \left(\frac{g_*}{100}\right)^{-\frac{1}{3}} \left(\frac{f}{f_{\text{sw}}}\right)^3 \left(\frac{7}{4 + 3(f/f_{\text{sw}})^2}\right)^{7/2}, \quad (\text{C.1})$$

where the peak frequency as observed today is given by

$$f_{\text{sw}} = 1.9 \times 10^{-5} \frac{1}{v_w} \left(\frac{\beta}{H_*}\right) \left(\frac{T_*}{100 \text{ GeV}}\right) \left(\frac{g_*}{100}\right)^{1/6} \text{ Hz}, \quad (\text{C.2})$$

⁶While this manuscript was being finalized, the code `WallGo` was released [80], which facilitates an accurate determination of the wall velocity and promises to reduce the uncertainty significantly in follow-up works.

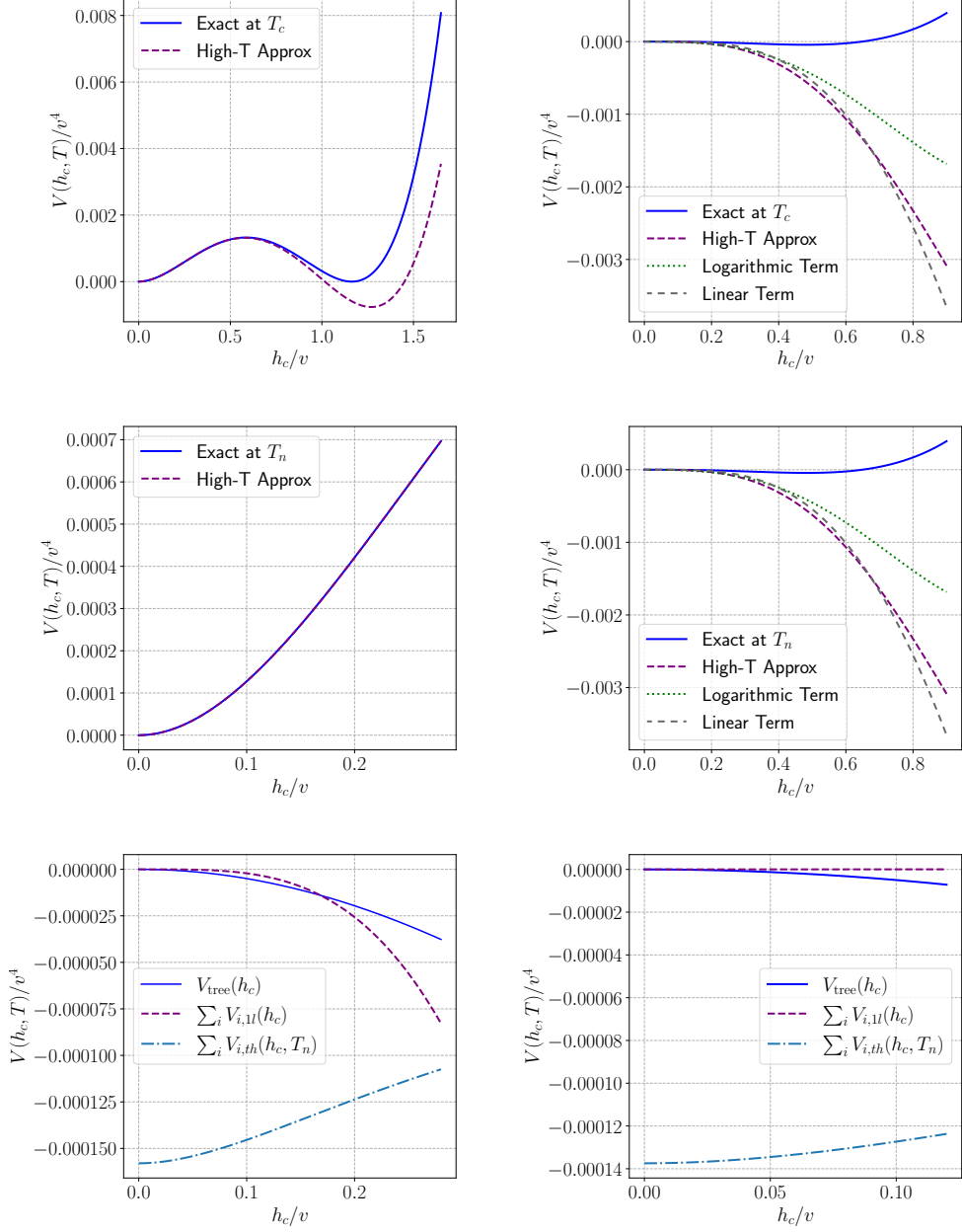


Figure 4. The effective potential $V(h_c, T)$, Eq. (2.15), including 1-loop corrections and thermal corrections. On the left-hand side we show the results for BP2 of Tab. 1, and on the right-hand side we show the results of BP5, Tab. 2. BP2 corresponds to a case without fermions, while for BP5 one fermion pair is added. The top plots correspond to a comparison of the exact thermal corrections as given by the integral functions defining J_b and J_f in Eq. (A.2) at T_c . The middle plots show the same comparison at T_n . The bottom plots show the individual contributions to the effective potential at T_n . We see that while for the case of no fermions present in the model, the high-temperature approximation gives an idea of the exact behavior, when fermions are present instead this approximation is not good, as the temperature corrections are dominated by the logarithmic term and to some extent the linear term.

the factor $\tau_{\text{sw}} = \min\left[\frac{1}{H_*}, \frac{R_*}{\bar{U}_f}\right]$ is the time scale of the duration of the phase transition [15, 59], and g_* and H_* , respectively, are the number of degrees of freedom and the Hubble parameter at the time of GW production in the thermal bath. In the non-runaway bubble case, the reheating temperature and the thermal bath temperature, T_* , coincide with the nucleation temperature T_n .⁷ Note that τ_{sw} can be either $1/H_*$ or R_*/\bar{U}_f , where $H_*R_* = \max(v_w, c_s)(8\pi)^{1/3}(\beta/H_*)^{-1}$. The root-mean-square (RMS) fluid velocity can be approximated as

$$\bar{U}_f^2 \approx \frac{3}{4} \left(\frac{\kappa_\nu \alpha}{1 + \alpha} \right).$$

We recall that the simulations on which Eq. (C.1) is based were restricted to values of $\alpha \lesssim 0.1$ and $\bar{U}_f \lesssim 0.05$ [81, 82]. The efficiency factor κ_ν can be approximated by [83]

$$\kappa_\nu \simeq \begin{cases} \alpha(0.73 + 0.83\sqrt{\alpha} + \alpha)^{-1}, & v_w \sim 1, \\ v_w^{6/5} 6.9\alpha(1.36 - 0.037\sqrt{\alpha} + \alpha)^{-1}, & v_w \ll 1. \end{cases} \quad (\text{C.3})$$

The MHD turbulence in the plasma is the sub-leading source of GW signals, with the energy density being given by

$$\Omega_{\text{turb}} h^2(f) = 3.35 \times 10^{-4} \left(\frac{\beta}{H_*} \right)^{-1} v_w \left(\frac{\epsilon \kappa_\nu \alpha}{1 + \alpha} \right)^{\frac{3}{2}} \left(\frac{g_*}{100} \right)^{-\frac{1}{3}} \frac{(f/f_{\text{turb}})^3 (1 + f/f_{\text{turb}})^{-\frac{11}{3}}}{1 + 8\pi \frac{f}{h_*}} \quad (\text{C.4})$$

with

$$h_* = 16.5 \frac{T_*}{10^8 \text{ GeV}} \left(\frac{g_*}{100} \right)^{1/6} \text{ Hz} \quad (\text{C.5})$$

and the peak frequency

$$f_{\text{turb}} = 2.7 \times 10^{-5} \frac{1}{v_w} \left(\frac{\beta}{H_*} \right) \left(\frac{T_*}{100 \text{ GeV}} \right) \left(\frac{g_*}{100} \right)^{1/6} \text{ Hz}. \quad (\text{C.6})$$

We have assumed that the turbulence factor κ_t can be written as $\kappa_t = \epsilon \kappa_\nu$, ϵ being another efficiency factor. The simulations in [56] suggest that only at most 5% to 10% of the bulk motion from the bubble wall is converted into vorticity, which enters into the turbulence contribution. Then it is customary to assume a conservative value of $\epsilon = 0.05$ [81].

The bubble wall velocity v_w must be derived from a microphysical description of the interactions between the background scalar field evolving through the bubble wall and the thermal plasma. Since this process is in general quite challenging, we present the GW density profiles for three values of v_w : 0.1, 1.0 and v_w^d . Here v_w^d is the detonation velocity $v_w^d = (1/\sqrt{3} + \sqrt{\alpha^2 + 2\alpha/3})/(1 + \alpha)$ [84]. The values for $\epsilon = 0.05$, $\bar{U}_f \sim 0.05$ were obtained in the regime of detonations and small α -deflagrations [56, 81, 82, 85].

A further, subdominant, source of GW is the collision of bubbles. An analytical expression based on simulations [86] is

$$\Omega_c h^2(f) = 5.01 \times 10^{-6} \left(\frac{g_*}{100} \right)^{-\frac{1}{3}} v_w^2 \left(\frac{\beta}{H_*} \right)^{-2} \left(\frac{\kappa_{\text{col}} \alpha}{1 + \alpha} \right)^2 \left(\frac{f}{f_{\text{col}}} \right)^3 \left(1 + 2 \left(\frac{f}{f_{\text{col}}} \right)^{2.07} \right)^{-2.18}. \quad (\text{C.7})$$

⁷Recalling that $T_{\text{rh}} \approx T_n(1 + \alpha)^{1/4}$ [59], so this is valid only for small values of α .

The efficiency factor κ_{col} is more involved than other efficiency factors as it depends on the type of barrier and the model that produces the FOPT [86].

Yet another subdominant contribution in the case of the non-runaway bubbles is the contribution from the scalar field. The expressions of this contribution have been estimated using simulations in the envelope approximation [87] and in the thin-wall and envelope approximations [88]. Another way is to compute it analytically in terms of the two-point correlator of the energy-momentum tensor [89], which yields

$$\Omega_\phi h^2(f_{\text{peak}}) \simeq 1.67 \times 10^{-5} \kappa_\phi^2 \Delta_{\text{peak}} \left(\frac{\beta}{H_*}\right)^{-2} \left(\frac{\alpha}{1+\alpha}\right)^2 \left(\frac{g_*}{100}\right)^{-\frac{1}{3}}, \quad (\text{C.8})$$

where

$$\Delta_{\text{peak}} = \frac{0.48 v_w^3}{1 + 5.3 v_w^2 + 5.0 v_w^4}. \quad (\text{C.9})$$

Both the bubble collision and the scalar field contributions are proportional to $(\beta/H_*)^{-2}$ and therefore suppressed with respect to the sound wave and turbulence contributions. Hence, we have not included these contributions in our numerical analysis.

References

- [1] R. Roshan and G. White, *Using gravitational waves to see the first second of the Universe*, [2401.04388](#).
- [2] F.L. Bezrukov and M. Shaposhnikov, *The Standard Model Higgs boson as the inflaton*, *Phys. Lett. B* **659** (2008) 703 [[0710.3755](#)].
- [3] T. Futamase and M. Tanaka, *Chaotic inflation with running nonminimal coupling*, *Phys. Rev. D* **60** (1999) 063511 [[hep-ph/9704303](#)].
- [4] S.C. Park and S. Yamaguchi, *Inflation by non-minimal coupling*, *JCAP* **08** (2008) 009 [[0801.1722](#)].
- [5] Y. Hamada, H. Kawai, K.-y. Oda and S.C. Park, *Higgs Inflation is Still Alive after the Results from BICEP2*, *Phys. Rev. Lett.* **112** (2014) 241301 [[1403.5043](#)].
- [6] Y. Hamada, H. Kawai, K.-y. Oda and S.C. Park, *Higgs inflation from Standard Model criticality*, *Phys. Rev. D* **91** (2015) 053008 [[1408.4864](#)].
- [7] X.-m. Zhang, *Operator analysis for the Higgs potential and cosmological bound on the Higgs-boson mass*, *Phys. Rev. D* **47** (1993) 3065 [[hep-ph/9301277](#)].
- [8] C. Grojean, G. Servant and J.D. Wells, *First-order electroweak phase transition in the standard model with a low cutoff*, *Phys. Rev. D* **71** (2005) 036001 [[hep-ph/0407019](#)].
- [9] D. Bödeker, L. Fromme, S.J. Huber and M. Seniuch, *The Baryon asymmetry in the standard model with a low cut-off*, *JHEP* **02** (2005) 026 [[hep-ph/0412366](#)].
- [10] C. Delaunay, C. Grojean and J.D. Wells, *Dynamics of Non-renormalizable Electroweak Symmetry Breaking*, *JHEP* **04** (2008) 029 [[0711.2511](#)].
- [11] B. Grinstein and M. Trott, *Electroweak Baryogenesis with a Pseudo-Goldstone Higgs*, *Phys. Rev. D* **78** (2008) 075022 [[0806.1971](#)].
- [12] P.H. Damgaard, A. Haarr, D. O’Connell and A. Tranberg, *Effective Field Theory and Electroweak Baryogenesis in the Singlet-Extended Standard Model*, *JHEP* **02** (2016) 107 [[1512.01963](#)].
- [13] J. de Vries, M. Postma, J. van de Vis and G. White, *Electroweak Baryogenesis and the Standard Model Effective Field Theory*, *JHEP* **01** (2018) 089 [[1710.04061](#)].

- [14] M. Chala, C. Krause and G. Nardini, *Signals of the electroweak phase transition at colliders and gravitational wave observatories*, *JHEP* **07** (2018) 062 [[1802.02168](#)].
- [15] J. Ellis, M. Lewicki, J.M. No and V. Vaskonen, *Gravitational wave energy budget in strongly supercooled phase transitions*, *JCAP* **06** (2019) 024 [[1903.09642](#)].
- [16] Y. Ema, *Higgs Scalon Mixed Inflation*, *Phys. Lett. B* **770** (2017) 403 [[1701.07665](#)].
- [17] D. Gorbunov and A. Tokareva, *Scaloron the healer: removing the strong-coupling in the Higgs- and Higgs-dilaton inflations*, *Phys. Lett. B* **788** (2019) 37 [[1807.02392](#)].
- [18] A. Salvio and A. Mazumdar, *Classical and Quantum Initial Conditions for Higgs Inflation*, *Phys. Lett. B* **750** (2015) 194 [[1506.07520](#)].
- [19] D.Y. Cheong, S.M. Lee and S.C. Park, *Primordial black holes in Higgs- R^2 inflation as the whole of dark matter*, *JCAP* **01** (2021) 032 [[1912.12032](#)].
- [20] D.Y. Cheong, K. Kohri and S.C. Park, *The inflaton that could: primordial black holes and second order gravitational waves from tachyonic instability induced in Higgs- R^2 inflation*, *JCAP* **10** (2022) 015 [[2205.14813](#)].
- [21] M. Colpi et al., *LISA Definition Study Report*, [2402.07571](#).
- [22] M. Maggiore et al., *Science Case for the Einstein Telescope*, *JCAP* **03** (2020) 050 [[1912.02622](#)].
- [23] M. Evans et al., *A Horizon Study for Cosmic Explorer: Science, Observatories, and Community*, [2109.09882](#).
- [24] S. Kawamura et al., *Current status of space gravitational wave antenna DECIGO and B-DECIGO*, *PTEP* **2021** (2021) 05A105 [[2006.13545](#)].
- [25] G.M. Harry, W. Folkner, P. Fritschel, E.S. Phinney and D.A. Shaddock, *The big bang observer: High laser power for gravitational wave astrophysics*, in *2007 Conference on Lasers and Electro-Optics (CLEO)*, pp. 1–1, 2007, [DOI](#).
- [26] A. Azatov, D. Barducci and F. Sgarlata, *Gravitational traces of broken gauge symmetries*, *JCAP* **07** (2020) 027 [[1910.01124](#)].
- [27] A. Bhoonah, J. Bramante, S. Nerval and N. Song, *Gravitational Waves From Dark Sectors, Oscillating Inflatons, and Mass Boosted Dark Matter*, *JCAP* **04** (2021) 043 [[2008.12306](#)].
- [28] E. Madge, E. Morgante, C. Puchades-Ibáñez, N. Ramberg, W. Ratzinger, S. Schenk et al., *Primordial gravitational waves in the nano-Hertz regime and PTA data — towards solving the GW inverse problem*, *JHEP* **10** (2023) 171 [[2306.14856](#)].
- [29] A. Addazi, Y.-F. Cai, A. Marciano and L. Visinelli, *Have pulsar timing array methods detected a cosmological phase transition?*, *Phys. Rev. D* **109** (2024) 015028 [[2306.17205](#)].
- [30] G. Arcadi, G.C. Dorsch, J.P. Neto, F.S. Queiroz and Y.M. Oviedo-Torres, *Probing a dark sector with collider physics, direct detection, and gravitational waves*, *Phys. Lett. B* **848** (2024) 138382 [[2307.06376](#)].
- [31] A. Chikaballi, K. Kowalska and E.M. Sessolo, *Naturally small neutrino mass with asymptotic safety and gravitational-wave signatures*, *JHEP* **11** (2023) 224 [[2308.06114](#)].
- [32] K. Hashino, M. Kakizaki, S. Kanemura, P. Ko and T. Matsui, *Gravitational waves from first order electroweak phase transition in models with the $U(1)_X$ gauge symmetry*, *JHEP* **06** (2018) 088 [[1802.02947](#)].
- [33] P. Schwaller, *Gravitational Waves from a Dark Phase Transition*, *Phys. Rev. Lett.* **115** (2015) 181101 [[1504.07263](#)].
- [34] J. Jaeckel, V.V. Khoze and M. Spannowsky, *Hearing the signal of dark sectors with gravitational wave detectors*, *Phys. Rev. D* **94** (2016) 103519 [[1602.03901](#)].

- [35] D. Borah, A. Dasgupta and S.K. Kang, *Gravitational waves from a dark $U(1)D$ phase transition in light of NANOGrav 12.5 yr data*, *Phys. Rev. D* **104** (2021) 063501 [[2105.01007](#)].
- [36] J.B. Dent, B. Dutta, S. Ghosh, J. Kumar and J. Runburg, *Sensitivity to dark sector scales from gravitational wave signatures*, *JHEP* **08** (2022) 300 [[2203.11736](#)].
- [37] A. Ashoorioon, *Exit from Inflation with a First-Order Phase Transition and a Gravitational Wave Blast*, *Phys. Lett. B* **747** (2015) 446 [[1502.00556](#)].
- [38] I. Masina and M. Quiros, *Electroweak metastability and Higgs inflation*, *Eur. Phys. J. C* **84** (2024) 1153 [[2403.02461](#)].
- [39] T. Tenkanen, K. Tuominen and V. Vaskonen, *A Strong Electroweak Phase Transition from the Inflaton Field*, *JCAP* **09** (2016) 037 [[1606.06063](#)].
- [40] S. Baek, J. Kersten, P. Ko and L. Velasco-Sevilla, *An unfamiliar way to generate the hierarchy of standard model fermion masses*, *JHEP* **02** (2024) 143 [[2309.07788](#)].
- [41] F. Staub, *SARAH*, [0806.0538](#).
- [42] F. Staub, *SARAH 4: A tool for (not only SUSY) model builders*, *Comput. Phys. Commun.* **185** (2014) 1773 [[1309.7223](#)].
- [43] S.R. Coleman and E.J. Weinberg, *Radiative Corrections as the Origin of Spontaneous Symmetry Breaking*, *Phys. Rev. D* **7** (1973) 1888.
- [44] L. Dolan and R. Jackiw, *Symmetry behavior at finite temperature*, *Phys. Rev. D* **9** (1974) 3320.
- [45] A.D. Linde, *Decay of the False Vacuum at Finite Temperature*, *Nucl. Phys. B* **216** (1983) 421.
- [46] F. Bezrukov, *The Higgs field as an inflaton*, *Class. Quant. Grav.* **30** (2013) 214001 [[1307.0708](#)].
- [47] I. Cheon et al., *Dictionary of FOPT for $SU(N)$ theories (to appear)*, .
- [48] S.J. Huber and T. Konstandin, *Gravitational Wave Production by Collisions: More Bubbles*, *JCAP* **09** (2008) 022 [[0806.1828](#)].
- [49] M. Hindmarsh, S.J. Huber, K. Rummukainen and D.J. Weir, *Gravitational waves from the sound of a first order phase transition*, *Phys. Rev. Lett.* **112** (2014) 041301 [[1304.2433](#)].
- [50] M. Hindmarsh, S.J. Huber, K. Rummukainen and D.J. Weir, *Numerical simulations of acoustically generated gravitational waves at a first order phase transition*, *Phys. Rev. D* **92** (2015) 123009.
- [51] A. Kosowsky, A. Mack and T. Kahniashvili, *Gravitational radiation from cosmological turbulence*, *Phys. Rev. D* **66** (2002) 024030 [[astro-ph/0111483](#)].
- [52] A. Nicolis, *Relic gravitational waves from colliding bubbles and cosmic turbulence*, *Class. Quant. Grav.* **21** (2004) L27 [[gr-qc/0303084](#)].
- [53] C. Caprini and R. Durrer, *Gravitational waves from stochastic relativistic sources: Primordial turbulence and magnetic fields*, *Phys. Rev. D* **74** (2006) 063521 [[astro-ph/0603476](#)].
- [54] T. Kahniashvili, A. Brandenburg, L. Campanelli, B. Ratra and A.G. Tevzadze, *Evolution of inflation-generated magnetic field through phase transitions*, *Phys. Rev. D* **86** (2012) 103005.
- [55] L. Kisslinger and T. Kahniashvili, *Polarized Gravitational Waves from Cosmological Phase Transitions*, *Phys. Rev. D* **92** (2015) 043006 [[1505.03680](#)].
- [56] M. Hindmarsh, S.J. Huber, K. Rummukainen and D.J. Weir, *Numerical simulations of acoustically generated gravitational waves at a first order phase transition*, *Phys. Rev. D* **92** (2015) 123009 [[1504.03291](#)].
- [57] C. Caprini, R. Durrer and G. Servant, *The stochastic gravitational wave background from turbulence and magnetic fields generated by a first-order phase transition*, *JCAP* **12** (2009) 024 [[0909.0622](#)].

- [58] P. Binetruy, A. Bohe, C. Caprini and J.-F. Dufaux, *Cosmological Backgrounds of Gravitational Waves and eLISA/NGO: Phase Transitions, Cosmic Strings and Other Sources*, *JCAP* **06** (2012) 027 [[1201.0983](#)].
- [59] J. Ellis, M. Lewicki and J.M. No, *On the Maximal Strength of a First-Order Electroweak Phase Transition and its Gravitational Wave Signal*, *JCAP* **04** (2019) 003 [[1809.08242](#)].
- [60] R. Jinno, T. Konstandin, H. Rubira and I. Stomberg, *Higgsless simulations of cosmological phase transitions and gravitational waves*, *JCAP* **02** (2023) 011 [[2209.04369](#)].
- [61] LIGO SCIENTIFIC, VIRGO collaboration, *Search for the isotropic stochastic background using data from Advanced LIGO's second observing run*, *Phys. Rev. D* **100** (2019) 061101.
- [62] L. Badurina et al., *AION: An Atom Interferometer Observatory and Network*, *JCAP* **05** (2020) 011 [[1911.11755](#)].
- [63] e. Amaro-Seoane, Pau, *Laser Interferometer Space Antenna*, *arXiv e-prints* (2017) [[1702.00786](#)].
- [64] Y.-B. Bae, C. Park, E.J. Son, S.-H. Ahn, M. Jeong, G. Kang et al., *A superconducting tensor detector for mid-frequency gravitational waves: Its multichannel nature and main astrophysical targets*, *Progress of Theoretical and Experimental Physics* **2024** (2024) 053E01 [<https://academic.oup.com/ptep/article-pdf/2024/5/053E01/57527315/ptae045.pdf>].
- [65] N. Herman, L. Lehoucq and A. Fúzfa, *Electromagnetic antennas for the resonant detection of the stochastic gravitational wave background*, *Phys. Rev. D* **108** (2023) 124009 [[2203.15668](#)].
- [66] L. Pagano, L. Salvati and A. Melchiorri, *New constraints on primordial gravitational waves from Planck 2015*, *Phys. Lett. B* **760** (2016) 823 [[1508.02393](#)].
- [67] T.C.C. et. al., *Core (cosmic origins explorer) a white paper*, 2011.
- [68] R.L. et. al., *Euclid definition study report*, 2011.
- [69] PLANCK collaboration, *Planck 2018 results. X. Constraints on inflation*, *Astron. Astrophys.* **641** (2020) A10 [[1807.06211](#)].
- [70] C.P. Burgess, H.M. Lee and M. Trott, *Power-counting and the Validity of the Classical Approximation During Inflation*, *JHEP* **09** (2009) 103 [[0902.4465](#)].
- [71] J.L.F. Barbon and J.R. Espinosa, *On the Naturalness of Higgs Inflation*, *Phys. Rev. D* **79** (2009) 081302 [[0903.0355](#)].
- [72] R.N. Lerner and J. McDonald, *Higgs Inflation and Naturalness*, *JCAP* **04** (2010) 015 [[0912.5463](#)].
- [73] E.J. Weinberg and A.-q. Wu, *Understanding complex perturbative effective potentials*, *Phys. Rev. D* **36** (1987) 2474.
- [74] D.E. Brahm, *Complex effective potentials and critical bubbles*, in *1st Yale-Texas Workshop on Baryon Number Violation at the Electroweak Scale*, 6, 1992 [[hep-ph/9206243](#)].
- [75] S.R. Coleman, *The Fate of the False Vacuum. 1. Semiclassical Theory*, *Phys. Rev. D* **15** (1977) 2929.
- [76] A. Linde, *Fate of the false vacuum at finite temperature: Theory and applications*, *Physics Letters B* **100** (1981) 37.
- [77] A. Ekstedt, O. Gould and J. Hirvonen, *BubbleDet: a Python package to compute functional determinants for bubble nucleation*, *JHEP* **12** (2023) 056 [[2308.15652](#)].
- [78] G.W. Anderson and L.J. Hall, *The Electroweak phase transition and baryogenesis*, *Phys. Rev. D* **45** (1992) 2685.

- [79] C.L. Wainwright, *CosmoTransitions: Computing Cosmological Phase Transition Temperatures and Bubble Profiles with Multiple Fields*, *Comput. Phys. Commun.* **183** (2012) 2006 [[1109.4189](#)].
- [80] A. Ekstedt et al., *How fast does the WallGo? A package for computing wall velocities in first-order phase transitions*, [2411.04970](#).
- [81] C. Caprini et al., *Science with the space-based interferometer eLISA. II: Gravitational waves from cosmological phase transitions*, *JCAP* **04** (2016) 001 [[1512.06239](#)].
- [82] C. Caprini et al., *Detecting gravitational waves from cosmological phase transitions with LISA: an update*, *JCAP* **03** (2020) 024.
- [83] J.R. Espinosa, T. Konstandin, J.M. No and G. Servant, *Energy Budget of Cosmological First-order Phase Transitions*, *JCAP* **06** (2010) 028 [[1004.4187](#)].
- [84] P.J. Steinhardt, *Relativistic detonation waves and bubble growth in false vacuum decay*, *Phys. Rev. D* **25** (1982) 2074.
- [85] M. Hindmarsh, S.J. Huber, K. Rummukainen and D.J. Weir, *Shape of the acoustic gravitational wave power spectrum from a first order phase transition*, *Phys. Rev. D* **96** (2017) 103520 [[1704.05871](#)].
- [86] D. Cutting, M. Hindmarsh and D.J. Weir, *Gravitational waves from vacuum first-order phase transitions: from the envelope to the lattice*, *Phys. Rev. D* **97** (2018) 123513 [[1802.05712](#)].
- [87] M. Kamionkowski, A. Kosowsky and M.S. Turner, *Gravitational radiation from first order phase transitions*, *Phys. Rev. D* **49** (1994) 2837 [[astro-ph/9310044](#)].
- [88] S.J. Huber and T. Konstandin, *Production of gravitational waves in the nMSSM*, *JCAP* **05** (2008) 017 [[0709.2091](#)].
- [89] R. Jinno and M. Takimoto, *Gravitational waves from bubble collisions: An analytic derivation*, *Phys. Rev. D* **95** (2017) 024009 [[1605.01403](#)].